

Integrin-Targeted Cyclic Forces Accelerate Neural Tube-Like Rosette Formation from Human Embryonic Stem Cells

Tuğba Topal, Zhenzhen Fan, Laura Y. Deng, Paul H. Krebsbach,* and Cheri X. Deng*

Mechanical forces play important roles in human embryonic stem cell (hESC) differentiation. To investigate the impact of dynamic mechanical forces on neural induction of hESCs, this study employs acoustic tweezing cytometry (ATC) to apply cyclic forces/strains to hESCs by actuating integrin-bound microbubbles using ultrasound pulses. Accelerated neural induction of hESCs is demonstrated as the result of combined action of ATC and neural induction medium (NIM). Specifically, application of ATC for 30 min followed by culture in NIM upregulates neuroectoderm markers Pax6 and Sox1 as early as 6 h after ATC, and induces neural tube-like rosette formation at 48 h after ATC. In contrast, no changes are observed in hESCs cultured in NIM without ATC treatment. In the absence of NIM, ATC application decreases Oct4, but does not increase Pax6 and Sox1 expression, nor does it induce neural rosette formation. The effects of ATC are abolished by inhibition of FAK, myosin activity, and RhoA/ROCK signaling. Taken together, the results reveal a synergistic action of ATC and NIM as an integrated mechanobiology mechanism that requires both integrin-targeted cyclic forces and chemical factors for accelerated neural induction of hESCs.

Human embryonic stem cells (hESCs), derived from the inner cell mass of pre-implementation embryos, are capable of differentiating into all three germ layers.^[1] Successful isolation and culture of hESCs in vitro have provided new opportunities for investigating basic stem cell biology and early human embryonic development. In particular, directed differentiation of hESCs has made it possible to generate specific cell types, opening up new frontiers for disease modeling, drug screening,

and cell replacement therapy. For example, recent demonstration that hESCs can be induced to differentiate and become motor neurons (MNs) offers unprecedented opportunity for studying MN development/function and developing cell-based therapies.^[2] However, current MN differentiation protocols, based on soluble factors and small molecules that inhibit and/or stimulate particular signaling pathways in defined culture conditions, not only are limited by low differentiation purity and yield, but also require prolonged cell culture that can take several weeks.^[3]


Mechanical forces are generated and transmitted across multiple scales, affecting cell fate during early embryonic development.^[4] It has been increasingly recognized that besides chemical factors, biomechanical and topographical cues also play critical roles in differentiation and self-renewal of hESCs.^[5] Thus new bioengineering tools and methods that leverage the intrinsic mechanosensitivity of hESCs may have the potential to improve hESC differentiation protocols.^[6] While static mechanical factors such as substrate stiffness have been shown to mediate hESC behavior including their differentiation,^[5] the effects of dynamic mechanical forces on hESCs have not been fully understood or exploited. This is due in part to the lack of appropriate techniques for applying dynamic forces to multiple cells in a high throughput fashion. Techniques such as atomic force microscopy (AFM)^[7] and optical tweezer, although capable of applying subcellular dynamic forces, are limited to single cell analysis and often require expensive instrumentation. Magnetic twisting cytometry (MTC),^[8] which uses functionalized magnetic microbeads attached to cells to apply forces to multiple cells, has been employed for microrheology and mechanobiology studies. However, solid microbeads are difficult to remove from cells, limiting post-MTC downstream assays and longitudinal studies that require continuous culture of cells devoid of exogenous materials.

Acoustic tweezing cytometry (ATC)^[9] is an ultrasound-based technique that utilizes ultrasound pulses to actuate encapsulated microbubbles (MBs) bound to integrin receptors to exert controlled forces to multiple cells simultaneously. MBs with stabilizing lipid or polymer shells (radius 1–3 μm) have been established as contrast agents for diagnostic ultrasound imaging^[10] and exploited for drug/gene delivery applications.^[11,12] Functionalization of MBs by decorating their shell

Dr. T. Topal, Dr. Z. Fan, Prof. P. H. Krebsbach, Prof. C. X. Deng
Department of Biomedical Engineering
University of Michigan
Ann Arbor, MI 48105, USA
E-mail: pkrebsbach@dentistry.ucla.edu; cxdeng@umich.edu

L. Y. Deng, Prof. C. X. Deng
Department of Mechanical Engineering
University of Michigan
Ann Arbor, MI 48109, USA

Dr. T. Topal, Prof. P. H. Krebsbach
Biointerfaces Institute
University of Michigan
Ann Arbor, MI 48109, USA
Prof. P. H. Krebsbach
UCLA School of Dentistry
Los Angeles, CA 90095, USA

 The ORCID identification number(s) for the author(s) of this article can be found under <https://doi.org/10.1002/adbi.201900064>.

DOI: 10.1002/adbi.201900064

with ligands to target specific cell membrane receptors enables ultrasound molecular imaging.^[13] These applications exploit the robust responses of MBs to ultrasound excitation.^[11,14] MBs expand and contract, or collapse when subjected to the periodic acoustic pressure of an ultrasound field. Volume expansion and contraction of MBs can generate microstreaming of surrounding fluid to exert shear stress on nearby cells, allowing probing cell deformability^[15] and manipulating single cells and organisms.^[16] In addition, a MB in an ultrasound field is also subjected to a net force, that is, the acoustic radiation force, due to momentum transfer from an ultrasound field.^[17] It is this acoustic radiation force that ATC utilizes to displace integrin-bound MBs without detachment, thereby applying a force/strain to cells via the MB-integrin-cytoskeleton (CSK) linkage. With a broadly applied ultrasound field with controlled parameters such as center frequency, acoustic pressure, pulse length, and pulse repetition frequency, ATC is capable of applying a defined force/strain to a large number of cells simultaneously with a subcellular resolution.^[9] Since gas filled MBs can be readily removed from the cells after ATC without leaving behind exogenous materials, and re-applied if needed for additional treatment, ATC provides an advantageous and biocompatible platform for mechanobiology applications.

Indeed, we have shown the utility of ATC for both cellular mechanical property characterization^[9,18,19] and generation of desirable mechanoresponses, including enhancement of osteogenic differentiation of mesenchymal stem cells^[20] and improvement of hESC survival.^[21] Particularly, we have recently demonstrated^[22] that application of integrin-targeted cyclic forces to hESCs for 30 min using ATC induced rapid down-regulation of E-cadherin as well as up-regulation of N-cadherin, Slug and Snail1, markers associated with epithelial-mesenchymal transition (EMT), suggesting that ATC induced exit of pluripotency and initiation of differentiation of hESCs.^[23]

Embryonic development involves a highly dynamic process with a spatiotemporally changing physical environment. Thus it is possible that the dynamic forces applied by ATC could provide potent mechanical cues to initiate hESC differentiation and EMT.^[22] Considering the changes in physical environment during development occur in the presence of soluble factors, this study is therefore motivated to leverage the novel capability of ATC to exploit the combined effects of integrin-targeted cyclic mechanical forces and biochemical factors for neural induction of hESCs.

This study utilized ATC to apply targeted mechanical force/strain to hESCs via functionalized MBs attached to the cells. In our experiments, MBs (SIMB4-5, Advanced Microbubble Laboratories, Boulder, CO) were decorated with RGD peptides targeting the $\alpha_v\beta_3$ integrin receptor of hESCs (Figure 1A,B). An ATC setup suitable for high-throughput application was implemented (Figure 1C), where a planar ultrasound transducer (center frequency 1 MHz) generated a series ultrasound pulses with defined acoustic pressure amplitudes, pulse duration, and pulse repetition frequency (Figure 1D). The ultrasound transducer, controlled by a computer-controlled positioning system, was submerged in a water tank to deliver the ultrasound pulses to the adherent cells at the Rayleigh distance of the transducer (55 mm) without direct contact with the cells/medium (Figure 1C). The transducer was set at a 45° angle to minimize

the interferences from direct reflections of ultrasound field and to displace the integrin-bound MBs on the surface of cells. As shown by real-time video-microscopic recording (Figure 1E; Figure S1, Movie S1, Supporting Information), integrin-bound MBs were moved by the acoustic radiation force associated with the applied ultrasound pulses. Without detachment, the displaced MBs retreated back toward their pre-ultrasound positions after each ultrasound pulse (Figure 1E; Movie S1, Supporting Information). While the time-dependent MB displacement and retraction curves can be used for cellular mechanical characterization,^[19] displacement of integrin-anchored MBs essentially induced distortion or stretching of the cellular structure or molecular assemblies within the cells via the MB-RGD-integrin-CSK linkage, thereby generating a strain to the underlining cells. Application of a series of ultrasound pulses generated cyclic MB displacement and cyclic strain to cells with an amplitude and frequency dependent on parameters such as the acoustic pressure and pulse repetition frequency.

To examine how ATC-induced displacement of integrin-anchored MBs affected hESCs, we measured the 5-pulse accumulative displacement of MBs as the sum of the net peak displacement achieved during each of the first five ultrasound pulses ($3.04 \pm 0.47 \mu\text{m}$, $n = 30$) and assessed the ensuing change of Oct4 expression in the cells. Comparison of the results from the ATC group (+MB+US) and control (–MB–US) revealed significant decrease of Oct4 expression in the cells treated by ATC (Figure 1F).

Displacement of integrin-bound MBs may infer the mechanical strain generated in the cells by ATC application. For example, a 5-pulse accumulative MB displacement of $3.04 \mu\text{m}$, corresponding to an average of displacement of $0.61 \mu\text{m}$ per ultrasound pulse, could suggest an overall strain of 6% to the cells, assuming an average length of $10 \mu\text{m}$ for the MB-RGD-integrin-CSK linkage. Of course, determination of the exact strain applied to the cells by ATC requires knowledge of the actual geometry and length of the MB-RGD-integrin-CSK linkage that was affected by ATC, which could not be readily obtained. In addition, ATC-induced stretch/deformation may not be uniformly distributed among the molecular assemblies within focal adhesions (FAs) and CSKs, making it difficult to determine precisely the strain distribution at the molecular level. Nevertheless, ATC-mediated displacement of integrin-anchored MBs is expected to generate molecular distortion and structural changes within the cells. Since force-induced structural change/functional modification has been recognized as a key factor in conversion of mechanical forces into biological signals in mechanotransduction,^[24] application of ATC may lead to functional modification of the focal adhesion and CSK proteins to impact hESC self-renewal or differentiation.

Therefore, this study was designed to leverage the capability of ATC-mediated cyclic forces/strains on hESCs and to investigate the combined action of ATC and NIM for neural induction of hESCs, as represented by expression of early neuroectoderm markers (Pax6 and Sox1) and formation of neural-like rosettes (Figure 1G).

During neural differentiation of hESCs, cells express Pax6 and Sox1^[25] and undergo morphogenetic events characterized by formation of radially organized cells described as “neural

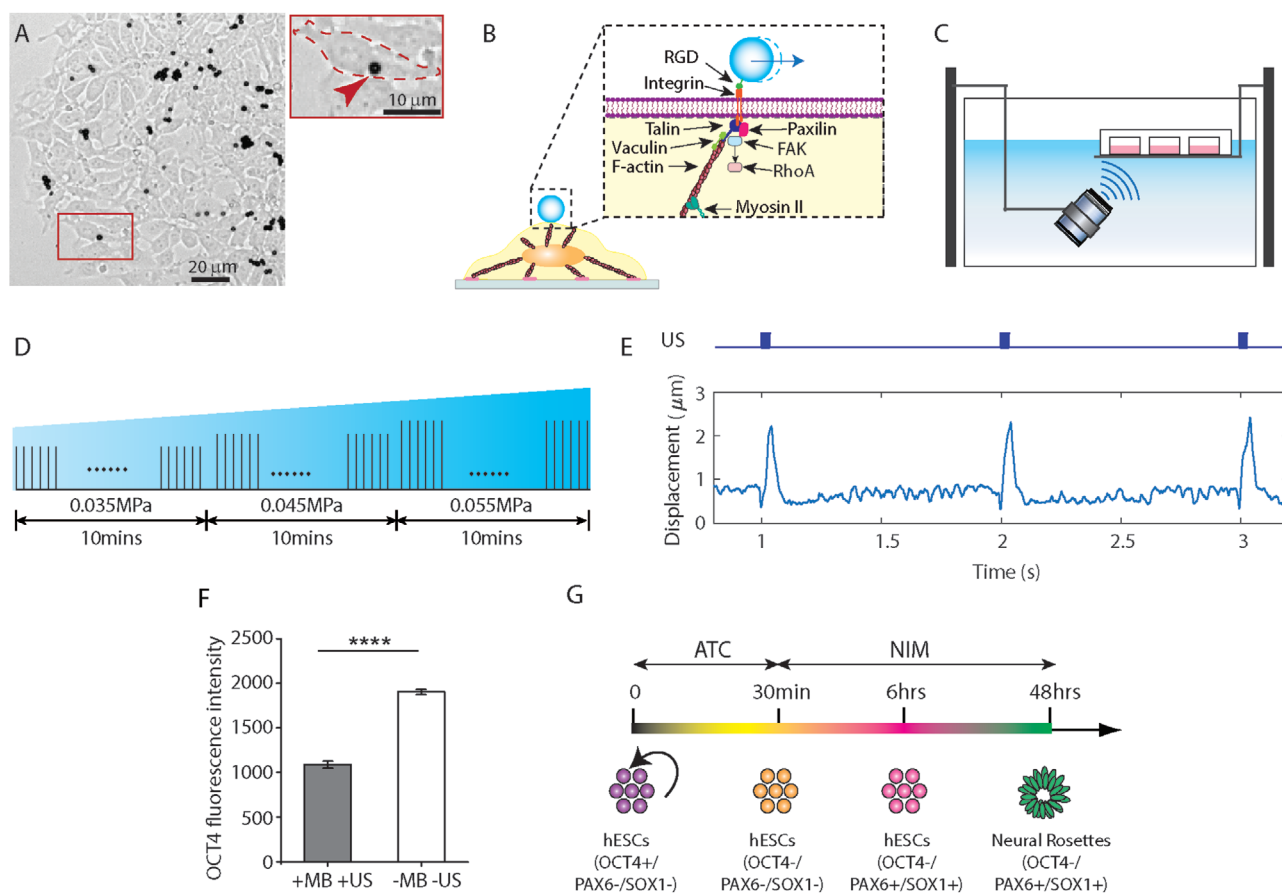


Figure 1. Application of acoustic tweezing cytometry (ATC) to hESCs using ultrasound (US) excitation of integrin-anchored microbubbles (MBs) to induce hESC neural differentiation. A) A bright field microscopic image showing targeted MBs attached to hESCs in a colony. Inset shows a single cell with an attached MB. B) An illustration of an integrin-bound MB via RGD-integrin binding subjected to the directional acoustic radiation force of ultrasound (US) pulses, exhibiting translational movement and exerting a defined strain to the cells via the integrin-focal adhesion-cytoskeleton linkage. C) Experiment setup for high through-put ATC application. D) US pulses used in ATC application. A total 30 min application of US pulses (pulse repetition frequency 1 Hz) was used, with the acoustic pressure increased every 10 min, from 0.035 MPa in the first 10 min, to 0.045 MPa the second 10 min, and to 0.055 MPa the last 10 min. E) Example of measured displacement of an integrin-bound MB during application of three US pulses. F) Fluorescence intensity of OCT4 expression in hESCs in ATC-group and control group in respectively. A total of 420 cells for the ATC group and 307 cells for control were analyzed. Experiments were conducted for at least $n = 3$. Mann-Whitney test (for non-normal distributed data) was used to compare the Oct4 intensity between these two conditions. $****p < 0.0001$. G) Experimental protocol for neural induction of hESCs by ATC application (30 min) followed by culture in NIM.

tube-like rosettes.^[26] Pax6 and Sox1 are early neuroectoderm markers and used to monitor neural induction. Neural rosettes, representing a developmental signature of neuroprogenitors derived from hESCs in vitro, recapitulate the molecular and morphogenetic sequence of events from gastrulation.^[27] Cells in this stage can differentiate into various region-specific neural cell types including MNs in response to appropriate cues.^[28]

We therefore conducted experiments to examine whether ATC application could regulate Pax6 and Sox1 expression. Our results from immunocytochemistry (ICC) analysis show that hESCs treated by ATC for 30 min followed by culture in NIM (+MB+US+NIM) exhibited decreased Oct4 expression, along with increased expression of both Pax6 and Sox1 as early as 6 h after ATC application (Figure 2A,B). ATC treatment also induced loss of cytoplasmic β -catenin, a transcriptional co-activator for regulation of gene expression.^[29] Detailed analysis of intracellular fluorescence signals revealed that, compared

to control cells without ATC treatment (-MB-US+NIM), about 50% of ATC-treated cells (+MB+US+NIM) exhibited decreased Oct4 along with increased Pax6 and Sox1 at this time point (Figure 2C,D). In contrast, no changes were observed in cells in the following three control groups: -MB-US+NIM (Figure 2A,B), -MB+US+NIM (Figure S2, Supporting Information), and +MB-US+NIM (Figure S2, Supporting Information), suggesting that NIM alone was insufficient to induce changes in transcription factor or neuroectoderm markers at this time point. On the other hand, in the absence of NIM, cells treated by ATC (+MB+US-NIM) exhibited decreased Oct4 expression, as observed previously,^[22] but showed no change in Pax6 and Sox1 expression (Figure 2E-H). Results of statistical analysis the four groups with NIM (Figure 2C; Figure S2C, Supporting Information) and two groups without NIM (Figure 2G) shown in Table S1, Supporting Information indicate that ATC induced statistically significant changes in Pax6 and Sox1 in the

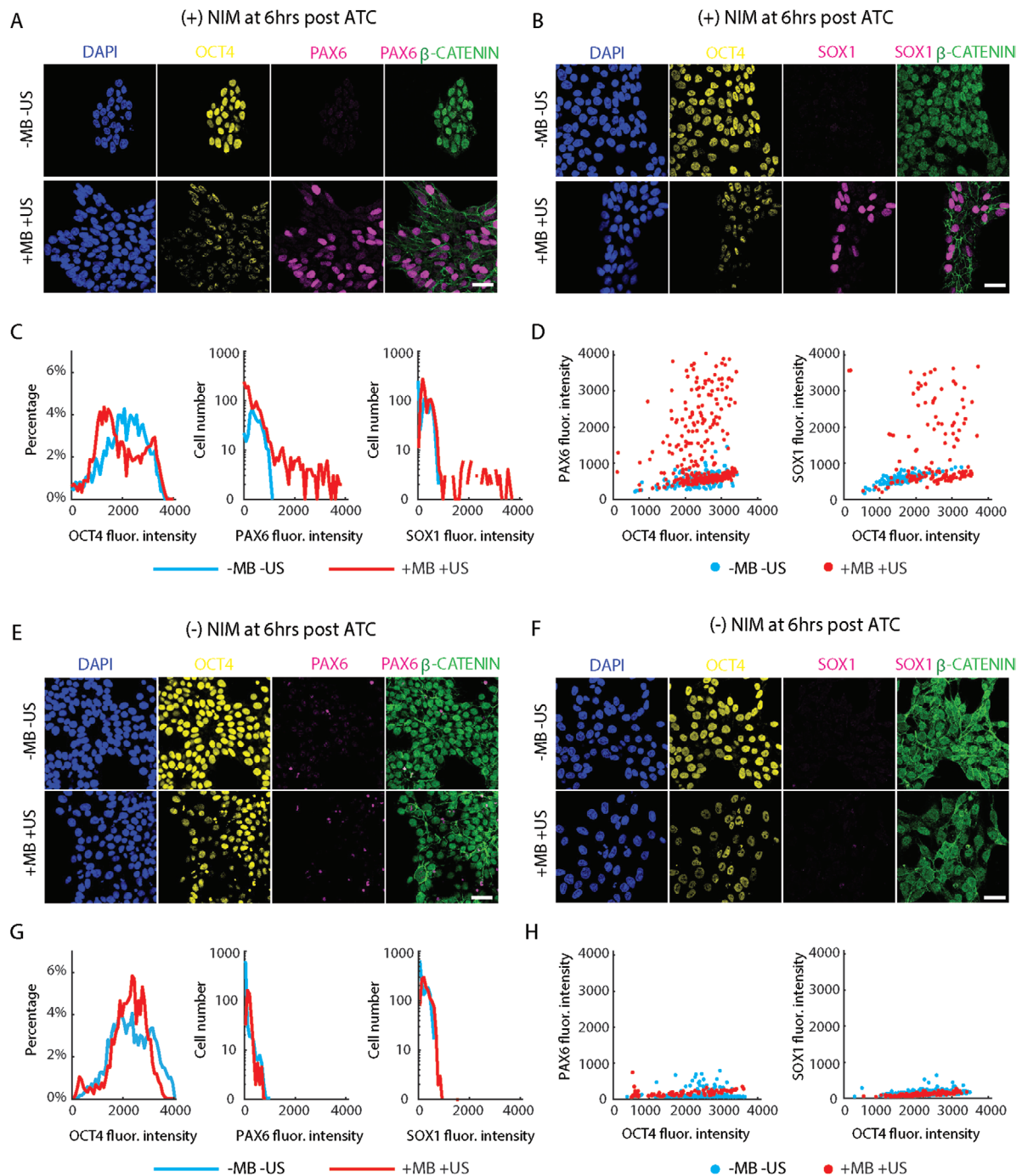


Figure 2. ATC treatment followed by 6-h culture in NIM decreased expression of OCT4, upregulated PAX6 and SOX1. A,B) Representative confocal immunocytochemical (ICC) fluorescence images showing protein expression in hESCs with (+MB+US) or without ATC treatment (–MB–US). Scale bar 50 μ m. C) Histograms of fluorescence intensity of OCT4, PAX6, and SOX1 in cells treated by ATC (+MB+US+NIM) and in cells without ATC (–MB–US+NIM). A total number of 2440 cells (+MB+US+NIM) and 1240 cells (–MB–US+NIM) from six independent experiments were analyzed for OCT4. A total number of 1376 cells (+MB+US+NIM) and 429 cells (–MB–US+NIM) from three independent experiments were analyzed for PAX6. A total number of 1064 cells (+MB+US+NIM) and 811 cells (–MB–US+NIM) from three independent experiments were analyzed for SOX1. D) Scatter plots of PAX6 versus OCT4 and SOX1 versus OCT4 for cells in +MB+US+NIM and –MB–US+NIM group. E, F) Representative ICC images showing that ATC (+MB+US) treatment in the absence of NIM decreased OCT4 in some hESCs. No increase in PAX6 or SOX1 was observed in both +MB+US–NIM and –MB–US–NIM group. Scale bar 50 μ m. G) Histograms of fluorescence intensity for OCT4, PAX6, and SOX1 in +MB+US–NIM and –MB–US–NIM group. A total of 1933 cells (+MB+US–NIM) and 2857 cells (–MB–US–NIM) from three independent experiments were analyzed for OCT4. A total of 586 cells (+MB+US–NIM) and 1292 cells (–MB–US–NIM) from three independent experiments were analyzed for PAX6. A total number of 1347 cells (+MB+US–NIM) and 1565 cells (–MB–US–NIM) from three independent experiments were analyzed for SOX1. H) Scatter plots of PAX6 versus OCT4, and SOX1 versus OCT4 for +MB+US–NIM and –MB–US–NIM group.

presence of NIM compared with the controls without ATC. In addition, ATC induced no changes in Pax6 and Sox1 in cells without NIM.

Although the ICC images show decreases in Oct4 in some cells at 6 h after ATC application with culture in NIM (Figure 2A,B), comparisons of the mean values reveal no statistically significant differences in Oct4 signals between the ATC group (+MB+US+NIM) and controls without ATC (–MB–US+NIM, +MB–US+NIM, and –MB+US+NIM) (Figure S2C, Table S1, Supporting Information). This is likely due to the heterogeneity in the cellular responses, as shown in the distribution of the Oct4 signals. Even though decreases were detected for some cells, the mean value from the overall population did not reflect such changes in the subpopulation of cells.

Taken together, our results show that the combined action of ATC and NIM induced upregulation of neuroectodermal markers Pax6 and Sox1 as early as 6 h. Either NIM (6-h culture) or ATC treatment (30 min) alone had no effect on either Pax6 or Sox1. Even though ATC alone, without NIM, initiated loss of Oct4 in some cells, upregulation of Pax6 and Sox1 required both ATC and NIM, suggesting an integrated mechanism involving both cyclic force/strain and chemical factors for neural induction of hESCs.

The ability of cells to sense and respond to mechanical signals is critical in development and relies on signaling pathways involving cell-ECM and cell-cell interaction. To determine how the effects of ATC on hESCs were associated with FAs and CSKs, we conducted experiments where cells were pre-treated for 30 min by either Blebbistatin (myosin II activity inhibitor), or FAK inhibitor, or Y-27632 (RhoA/ROCK signaling inhibitor) 1 h before ATC application. The cells were cultured in NIM for 6 h after ATC application. Results from immunocytochemistry (ICC) analysis show that the effects of ATC were abrogated by these drug treatments using Blebbistatin, FAK inhibitor, or Y-27632. No changes in expression of Oct4, Pax6 and Sox 1 were detected in these cells treated by ATC (+MB+US) (Figure S3, Supporting Information), suggesting that ATC-mediated upregulation of neuroectoderm markers (Figure 2) depended on mechanobiology pathways involving activation of focal adhesion components, actomyosin contractility (with myosin II), and Rho/ROCK signaling.

Following the observation of upregulated Pax6 and Sox1 expression after ATC treatment (for 30 min) and culture in NIM for 6 h, we conducted experiments to further examined the cells 48 h after ATC application. Excitingly, ATC treatment followed by 48-h culture in NIM induced the formation of neural rosettes, where significantly upregulated Pax6 and Sox1 expression was observed and accompanied by significant loss of Oct4 expression (Figure 3A,B). Compared to the results at 6 h post ATC treatment (Figure 2), almost all of the ATC-treated cells exhibited decreased Oct4, as well as upregulated Pax6 and Sox1 after 48-h culture in NIM (Figure 3C,D). In contrast, no changes in Oct4, Pax6, or Sox1 were detected in cells in the control groups –MB–US+NIM (Figure 3A–D), –MB+US+NIM (Figure S4, Supporting Information), and +MB–US+NIM (Figure S4, Supporting Information). On the other hand, in the absence of NIM, ATC treatment alone (+MB+US–NIM) decreased Oct4 expression, similarly as before (Figure 2E,F),^[22] but produced neither change in Pax6 and Sox1 expression nor

neural rosette formation (Figure 3E–H). Results of statistical analysis of the four groups with NIM (Figure 3C; Figure S4C, Supporting Information) and two groups without NIM (Figure 3G) shown in Table S2, Supporting Information, indicate that ATC induced statistically significant changes in Pax6 and Sox1 in the presence of NIM compared to controls without ATC. In addition, cells treated by ATC exhibited statistically significant decrease in Oct4 after 48 h without NIM (Table S2, Supporting Information; Figure 3A,B), but no changes in Pax6 and Sox1 were detected in the cells treated by ATC without NIM at 48 h.

These results suggest that combined action of the integrin-targeted cyclic forces/strains mediated by ATC and chemical factors in NIM facilitated neural induction of hESCs, signified by upregulation of neural-ectodermal markers and formation of neural rosettes after 48 h. Such rapid changes facilitated by ATC application is in great contrast with the typical time frame of 7–10 days needed for neural rosette formation when only soluble factors are used.^[30] The accelerated neural induction of hESCs by a short duration of ATC application suggests a unique mechanism of mechanotransduction in hESCs that involves integrin-targeted cyclic force/strain as a potent mechanical signal.

To further study the role of ATC in the observed rapid neural induction of hESCs, we performed reverse transcription quantitative real-time PCR (RT-qPCR) to examine the temporal profiles of expression of pluripotency (Nanog, Oct4, and Sox2) and neuro-ectodermal related genes (Pax6, Sox1, Nestin, Ap2a1, Ap2a2, and β III-Tubulin) in cells at 6, 24, and 48 h after 30 min ATC treatment.

Our results show that without the impact of ATC (–MB–US+NIM, –MB+US+NIM, +MB–US+NIM), cells did not exhibit changes in Nanog and Sox2 after culture in NIM (Figure 4A). In contrast, application of ATC followed by culture in NIM (+MB+US+NIM) induced changes in Nanog (at 6, 24, and 48 h) and Sox2 (at 24 and 48 h) (Figure 4A), suggesting disruption of the pluripotency transcription factor circuitry in these cells. Our RT-qPCR analysis did not reveal a significant decrease in Oct4 in cells treated by ATC and NIM, in contrast to our findings from ICC analysis (Figures 2 and 3). In addition, while decreased Nanog and increased Nestins were mostly reported in literature regarding neural differentiation of hESCs by soluble factors alone, the mechanisms of ATC induced neural differentiation of hESCs are unknown for us to pinpoint the causes of our observations.

Application of ATC followed by culture in NIM also resulted in notable changes in neuro-ectodermal gene expression (Figure 4B). Increased Sox1 was seen (at 6, 24, and 48 h) along with increased Pax6 (at 24 and 48 h), an observation generally in-line with our ICC results which show increases of both Pax6 and Sox1 at 6 h (Figure 2). Nestin and β III-Tubulin (Tubb3) appear to decrease in cells treated by ATC (+MB+US+NIM), but no significant changes in neural crest (NC) markers Ap2a1 and Ap2a2 were observed in cells treated by ATC and NIM (Figure 4B). Results of statistical analysis the four groups with NIM (Figure 4) are shown in Table S3, Supporting Information.

The differences between the RT-qPCR results and ICC results in this study could be attributed to factors associated with the specific mechanisms of the two techniques. RT-qPCR examines mRNA while ICC detects protein. Post-transcriptional and

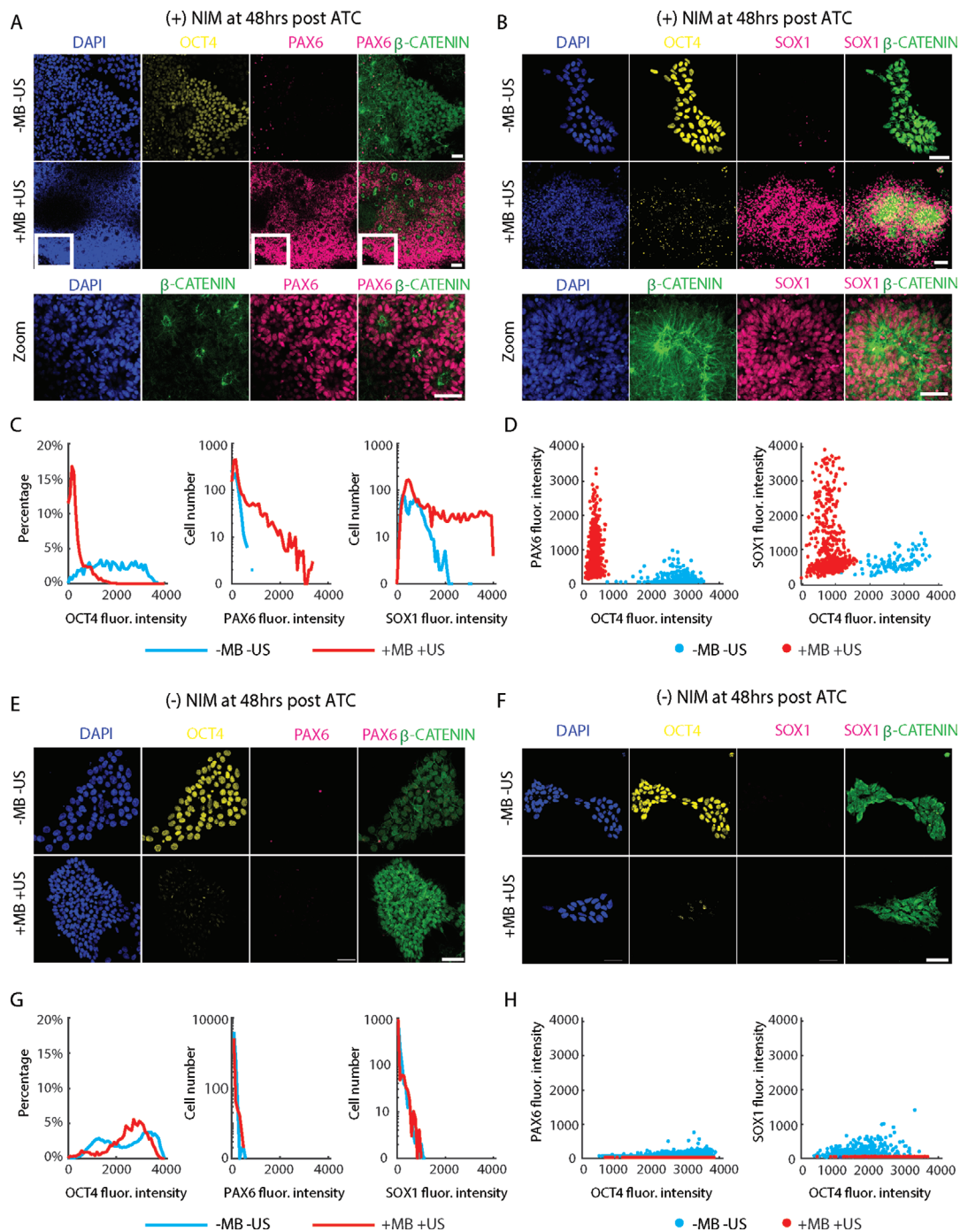


Figure 3. Application of ATC (30 min) followed by 48 h culture in NIM promotes neural rosettes formation. A,B) Representative ICC images showing that ATC treatment followed 48h culture in NIM upregulated PAX6 and SOX1 but decreased OCT4, along with formation of neural rosettes and membrane translocation of β -catenin. Scale bar 50 μ m. C) Histograms of OCT4, PAX6, and SOX1 fluorescence intensity for cells in +MB+US+NIM and -MB-US+NIM group. A total of 4413 cells (+MB+US+NIM) and 1708 cells (-MB-US+NIM) from six independent experiments were analyzed for OCT4. A total of 2244 cells (+MB+US+NIM) and 942 cells (-MB-US+NIM) from three independent experiments were analyzed for PAX6. A total of 2169 cells (+MB+US+NIM) and 766 cells (-MB-US+NIM) from three independent experiments were analyzed for SOX1. D) Scatter plots of PAX6 versus OCT4, and SOX1 versus OCT4 for +MB+US+NIM and -MB-US+NIM group. E,F) Representative ICC images showing that ATC (+MB+US) treatment in the absence of NIM resulted in decrease of OCT4 in a small number of hESCs. No PAX6 nor SOX1 upregulation was observed for +MB+US-NIM or -MB-US-NIM group. Scale bar 50 μ m. G) Histograms of OCT4, PAX6, and SOX1 fluorescence intensity for +MB+US-NIM and -MB-US-NIM group at 48 h. A total number of 3928 cells (+MB+US-NIM) and 6024 cells (-MB-US-NIM) from six independent experiments were analyzed for OCT4. A total of 2738 cells (+MB+US-NIM) and 4718 cells (-MB-US-NIM) from three independent experiments were analyzed for PAX6. A total of 1190 cells (+MB+US-NIM) and 1306 cells (-MB-US-NIM) from three independent experiments were analyzed for SOX1. H) Scatter plots of PAX6 versus OCT4, and SOX1 versus OCT4 for +MB+US-NIM and -MB-US-NIM group.

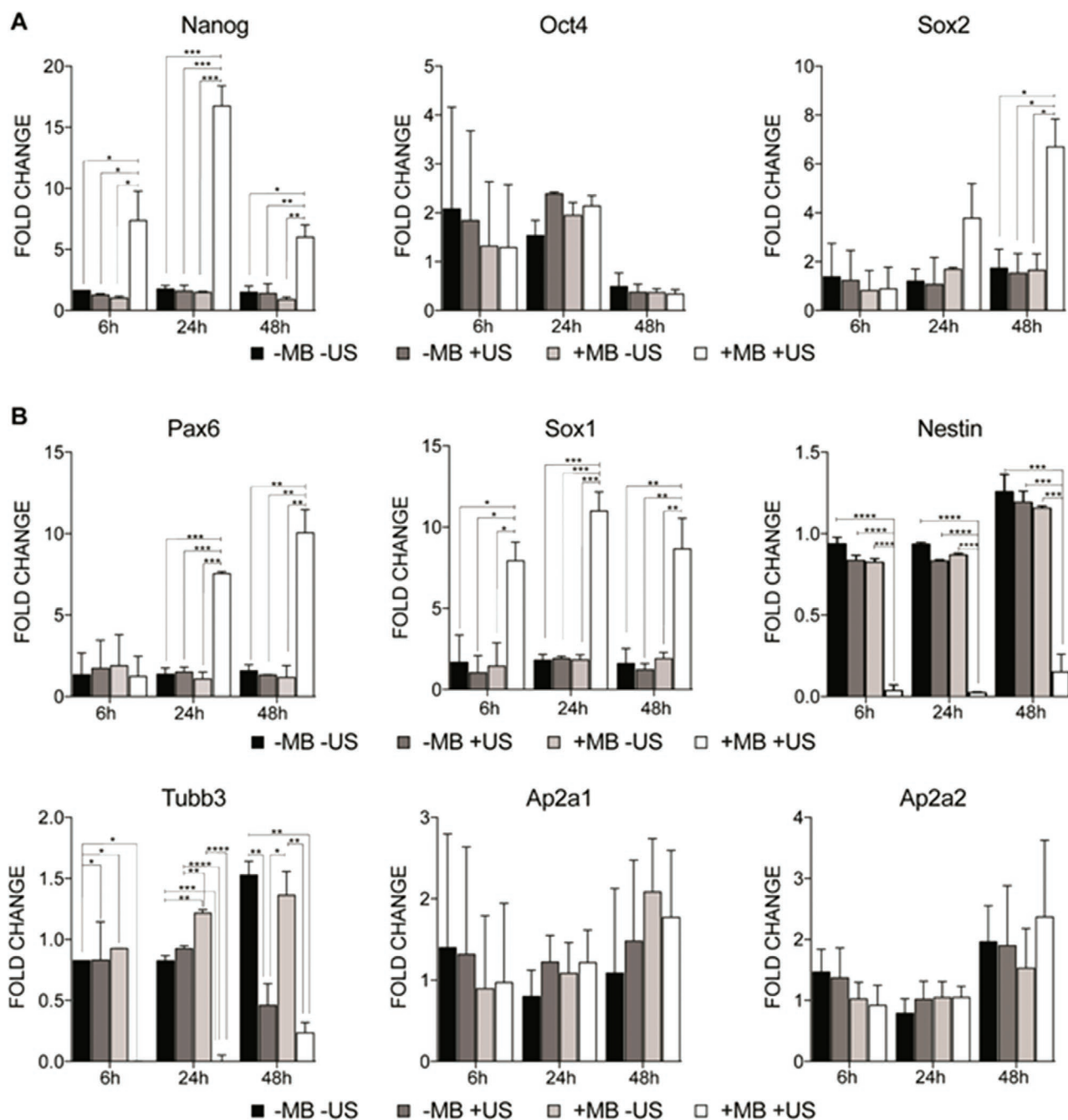


Figure 4. Relative transcript levels of pluripotency and neural genes from RT-qPCR analysis of cells in all groups (–MB–US, –MB+US, +MB–US, +MB+US) after ATC treatment followed by 6, 24, and 48 h culture in neural induction medium (NIM). A) Relative transcript levels of pluripotency genes (Nanog, Oct4, and Sox2) B) Relative transcript levels neuroectoderm transcription factors (Pax6, Sox1, Nestin, Tubb3, AP2a1, and Ap2a2). All data were normalized against *GAPDH* and the cells without microbubbles (MBs), ultrasound (US), and NIM (–MB–US–NIM), and plotted as the mean, with $n = 3$ independent experiments. One-way ANOVA-TUKEY multiple comparison test was performed for all groups in each panel. *: $p < 0.05$; **: $p < 0.01$; ***: $p < 0.001$; ****: $p < 0.0001$.

posttranslational regulation steps during the complex pathways from gene to protein may lead to a lack of correlation of transcription and translation outcomes,^[31] which could explain the observed discrepancy between RT-qPCR (mRNA) and ICC (protein) results in our study. In addition, in RT-qPCR, all cells were collected from an experiment for analysis, while ICC examined

individual cells and thus could clearly detect heterogeneity of response in the cell population. As shown in Figure 2, not all cells exhibited changes in protein expression for Oct4, Pax6, and Sox1 at 6 h after ATC application. The heterogeneity of this cell response could be due to intrinsic cell heterogeneity such that some cells respond to ATC stimulation earlier than

others. In addition, MBs attachment was not uniform for all cells (Figure 1A), and this may result in some inhomogeneity in the effect of ATC on individual cells. Thus when all cells were collected for RT-qPCR analysis, which measured the combined response of all cells present, response of the affected cells may go undetected against the background of nonresponsive cells in the population, particularly at the early time point of 6 h after ATC in our experiments.

Since not every cell was attached with MBs, it is reasonable to expect that the number of MBs/cell could be important in ATC induced neural differentiation with the ultimate goal of generating functional neurons with high purity and yield. However, our previous study has revealed that ATC generated a global and homogenous responses in all hESCs in a colony even though only a subpopulation of cells were attached with MBs, suggesting the contribution of cell-cell contacts/communication.^[22] In the current study, while not all cells exhibited changes in protein expression for Oct4, Pax6, and Sox1 at the early time point of 6 h after ATC (Figure 2), eventually almost all cells exhibited these changes at 48 h (Figure 3), suggesting again the role of cell-cell communication in cellular responses to ATC stimulation.

Taken together, these data demonstrate that ATC-mediated cyclic strain alters transcriptional activities in hESCs and initiates upregulation of Pax6 and Sox1 expression in the presence of biochemical cues. The results from both RT-qPCR and ICC analyses are generally consistent, especially when neural rosettes were formed and significantly increased Pax6 and Sox1 were detected 48 h after ATC application (Figure 3 and Figure 4B).

Compared to the results of neural rosettes induced by chemical factors alone, our results reveal differences in Pax6 and Sox1 expression, which may underscore the unique mechanism for the accelerated neural induction of hESCs by the combined action of ATC-mediated mechanical forces and soluble factors. For example, in the presence of growth factors and inhibitors (without mechanical forces), Pax6, but not Sox1, was expressed in neural rosettes at day 10,^[30] which was also a much longer time duration than the 48 h observed in our study. Another study showed that treatment with chemically defined medium supplemented with noggin generated Pax6+/Sox1- neural rosettes, while Pax6+/Sox1+ rosettes only formed after fibroblast growth factors such as FGF2 and FGF8 were supplemented.^[32]

Differentiation of hESCs into a specific cell lineage is a complex process involving multiple stages. Detailed understanding of this elaborate process may provide critical insights into early development and for cell therapies that require efficient methods for directed differentiation of hESCs in vitro. Leveraging the intrinsic mechanosensitivity of hESCs and the unique capability of ATC for applying integrin-targeted cyclic force/strain to hESCs, this study demonstrated that combined action of ATC and NIM accelerated upregulation of neuroectoderm markers and formation of neural rosettes. While our ultimate goal is to develop ATC for facilitating hESC neural differentiation to obtain fully functional MNs with high purity and yield, our objective in this study was to demonstrate the utility of ATC-mediated integrin-targeted cyclic force/strain in mechanobiology of hESCs. Results from this study not only highlight

the unique role of ATC in initiating hESC neural differentiation, but also reveal an integrated mechanism requiring both dynamic mechanical forces and chemical factors for accelerating neural differentiation of hESCs.

In this study, ATC was applied for 30 min to exert cyclic forces/strains to hESCs via the MB-integrin-CSK linkage by using ultrasound pulses with a defined pulse duration, pulse repetition frequency, and acoustic pressures. The ultrasound parameters used in this study need not be the only choices and may be optimized to further improve the outcome of neural induction of hESCs in future studies. Besides acoustic pressure and pulse duration, MB displacement could also be influenced by interactions among bubbles in close range of each other, due to the secondary acoustic radiation force as shown before.^[18] Thus, the number of MBs per cell will be another factor to consider even under the same ultrasound parameters.

Our measurements in this study show that the integrin-bound MBs were displaced without detachment, suggesting the role of the MB displacement in the decrease of Oct4 in the hESCs (Figure 1E,F) that could be related to the distortion/strain applied to the FA-CSK linkage of the cells subjected to ATC treatment. Although the exact mechanism of ATC-induced hESC differentiation remains to be shown, it is possible that ATC-induced distortion/strain to the FA-CSK linkage may expose protein binding sites responsible for mechanotransduction in hESCs.^[24]

We employed RT-qPCR and ICC in this study to evaluate the dynamic changes in mRNA expression and protein expression during neural differentiation of hESCs induced by ATC and NIM. RT-qPCR gives mRNA abundance but may not be directly indicative of protein abundance. On the other hand, ICC offers high spatial resolution and provides information regarding protein localization within each cell and co-expression with other proteins. ICC also identifies affected and unaffected cells, allowing assessment of inhomogeneity in cell responses. While beyond the scope of current study, future investigations are needed to evaluate correlation between mRNA expression and protein expression in ATC-induced accelerated neural differentiation of hESCs, and to determine the dynamic changes in expression of pluripotent genes and how they are related to the neural genes in the transition from a pluripotent cell to a neural-specific cell type.

Supporting Information

Supporting Information is available from the Wiley Online Library or from the author.

Acknowledgements

T.T. and Z.F. contributed equally to this work. This work was supported by the National Institutes of Health (R01 EB019436 to C. X. D.).

Conflict of Interest

The authors declare no conflict of interest.

Keywords

acoustic tweezing cytometry, cyclic force, human embryonic stem cell, neural differentiation, neural rosette

Received: March 11, 2019

Revised: July 29, 2019

Published online: August 21, 2019

- [1] J. A. Thomson, J. Itskovitz-Eldor, S. S. Shapiro, M. A. Waknitz, J. J. Swiergiel, V. S. Marshall, J. M. Jones, *Science* **1998**, 282, 1145.
- [2] a) X. J. Li, Z. W. Du, E. D. Zarnowska, M. Pankratz, L. O. Hansen, R. A. Pearce, S. C. Zhang, *Nat. Biotechnol.* **2005**, 23, 215; b) N. Singh Roy, T. Nakano, L. Xuing, J. Kang, M. Nedergaard, S. A. Goldman, *Experiment. Neurol.* **2005**, 196, 224; c) H. Lee, G. A. Shamy, Y. Elkabetz, C. M. Schofield, N. L. Harrision, G. Panagiotakos, N. D. Socci, V. Tabar, L. Studer, *Stem Cells* **2007**, 25, 1931.
- [3] a) M. E. Hester, M. J. Murtha, S. Song, M. Rao, C. J. Miranda, K. Meyer, J. Tian, G. Boulting, D. V. Schaffer, M. X. Zhu, S. L. Pfaff, F. H. Gage, B. K. Kaspar, *Mol Ther* **2011**, 19, 1905; b) B. Y. Hu, S. C. Zhang, *Nat Protoc* **2009**, 4, 1295; c) S. M. Chambers, C. A. Fasano, E. P. Papapetrou, M. Tomishima, M. Sadelain, L. Studer, *Nat Biotechnol* **2009**, 27, 275.
- [4] C. J. Chan, C. P. Heisenberg, T. Hiiragi, *Current Biol.* **2017**, 27, R1024.
- [5] a) Y. Sun, K. M. Yong, L. G. Villa-Diaz, X. Zhang, W. Chen, R. Philson, S. Weng, H. Xu, P. H. Krebsbach, J. Fu, *Nat. Mater.* **2014**, 13, 599; b) W. Chen, Y. Sun, J. Fu, *Small* **2013**, 9, 81.
- [6] Y. Sun, J. Fu, *ACS Chem. Neurosci.* **2014**, 5, 621.
- [7] R. D. Gonzalez-Cruz, V. C. Fonseca, E. M. Darling, *Proc. National Acad. Sci.* **2012**, 109, E1523.
- [8] a) N. Wang, J. P. Butler, D. E. Ingber, *Science* **1993**, 260, 1124; b) F. Chowdhury, S. Na, D. Li, Y.-C. Poh, T. S. Tanaka, F. Wang, N. Wang, *Nat. Mater.* **2010**, 9, 82.
- [9] Z. Fan, Y. Sun, C. Di, D. Tay, W. Chen, C. X. Deng, J. Fu, *Scientific Reports* **2013**, 3, 2176.
- [10] S. Qin, C. F. Caskey, K. W. Ferrara, *Phys. Med. Biol.* **2009**, 54, R27.
- [11] K. Ferrara, R. Pollard, M. Borden, *Annual Rev. Biomed. Eng.* **2007**, 9, 415.
- [12] S. Hernot, A. L. Klibanov, *Adv. Drug Delivery Rev.* **2008**, 60, 1153.
- [13] A. L. Klibanov, *J. Nuclear Cardiol.* **2007**, 14, 876.
- [14] a) C. X. Deng, F. L. Lizzi, *Ultrasound Med Biol* **2002**, 28, 277; b) Z. Fan, D. Chen, C. X. Deng, *Ultrasound Med Biol* **2014**, 40, 1260.
- [15] Y. Xie, N. Nama, P. Li, Z. Mao, P. H. Huang, C. Zhao, F. Costanzo, T. J. Huang, *Small* **2016**, 12, 902.
- [16] D. Ahmed, A. Ozcelik, N. Bojanala, N. Nama, A. Upadhyay, Y. Chen, W. Hanna-Rose, T. J. Huang, *Nature Commun.* **2016**, 7, 11085.
- [17] P. A. Dayton, J. S. Allen, K. W. Ferrara, *J. Acoust. Soc. Am.* **2002**, 112, 2183.
- [18] D. Chen, Y. Sun, M. S. Gudur, Y. S. Hsiao, Z. Wu, J. Fu, C. X. Deng, *Biophys. J.* **2015**, 108, 32.
- [19] Z. Fan, X. Xue, R. Perera, S. Nasr Esfahani, A. A. Exner, J. Fu, C. X. Deng, *Small* **2018**, 14, 1803137.
- [20] X. Xue, X. Hong, Z. Li, C. X. Deng, J. Fu, *Biomaterials* **2017**, 134, 22.
- [21] D. Chen, Y. Sun, C. X. Deng, J. Fu, *Biophys. J.* **2015**, 108, 1315.
- [22] T. Topal, X. Hong, X. Xue, Z. Fan, N. Kanetkar, J. T. Nguyen, J. Fu, C. X. Deng, P. H. Krebsbach, *Scientific Reports* **2018**, 8, 12977.
- [23] a) K. A. D'Amour, A. D. Agulnick, S. Eliazer, O. G. Kelly, E. Kroon, E. E. Baetge, *Nat Biotechnol* **2005**, 23, 1534; b) A. M. Eastham, H. Spencer, F. Soncin, S. Ritson, C. L. Merry, P. L. Stern, C. M. Ward, *Cancer Res* **2007**, 67, 11254.
- [24] a) A. del Rio, R. Perez-Jimenez, R. Liu, P. Roca-Cusachs, J. M. Fernandez, M. P. Sheetz, *Science* **2009**, 323, 638; b) X. Hu, F. M. Margadant, M. Yao, M. P. Sheetz, *Protein Sci* **2017**, 26, 1337.
- [25] a) A. L. Perrier, V. Tabar, T. Barberi, M. E. Rubio, J. Bruses, N. Topf, N. L. Harrison, L. Studer, *Proc Natl Acad Sci USA* **2004**, 101, 12543; b) D. M. Suter, D. Tirefort, S. Julien, K. H. Krause, *Stem Cells* **2009**, 27, 49.
- [26] S. C. Zhang, M. Wernig, I. D. Duncan, O. Brustle, J. A. Thomson, *Nature Biotechnol.* **2001**, 19, 1129.
- [27] Y. Elkabetz, G. Panagiotakos, G. Al Shamy, N. D. Socci, V. Tabar, L. Studer, *Genes Develop.* **2008**, 22, 152.
- [28] S. Shin, M. Mitalipova, S. Noggle, D. Tibbitts, A. Venable, R. Rao, S. L. Stice, *Stem Cells* **2006**, 24, 125.
- [29] X. Zhou, J. P. Chadarevian, B. Ruiz, Q. L. Ying, *Stem Cell Rep.* **2017**, 9, 732.
- [30] B. Y. Hu, J. P. Weick, J. Yu, L. X. Ma, X. Q. Zhang, J. A. Thomson, S. C. Zhang, *Proc. National Acad. Sci.* **2010**, 107, 4335.
- [31] A. Vilmar, J. Garcia-Foncillas, M. Huarritz, E. Santoni-Rugiu, J. B. Sorensen, *Lung Cancer* **2012**, 75, 306.
- [32] S. Yao, S. Chen, J. Clark, E. Hao, G. M. Beattie, A. Hayek, S. Ding, *Proc. National Acad. Sci.* **2006**, 103, 6907.